

Deep Neural Networks for Defects Detection in Gas Metal Arc Welding

Original

Deep Neural Networks for Defects Detection in Gas Metal Arc Welding / Nele, Luigi; Mattera, Giulio; Voza, Mario. - In: APPLIED SCIENCES. - ISSN 2076-3417. - 12:7(2022). [10.3390/app12073615]

Availability:

This version is available at: 11583/2994881 since: 2024-11-28T23:12:10Z

Publisher:

MDPI

Published

DOI:10.3390/app12073615

Terms of use:

This article is made available under terms and conditions as specified in the corresponding bibliographic description in the repository

Publisher copyright

(Article begins on next page)

Article

Deep Neural Networks for Defects Detection in Gas Metal Arc Welding

Luigi Nele ^{1,*}, Giulio Mattera ¹  and Mario Vozza ²

¹ Department of Chemical, Materials and Industrial Manufacturing Engineering, University of Naples Federico II, 80125 Naples, Italy; giulio.mattera@unina.it

² National Research Council, Institute of Nanostructured Materials (ISMN), 40129 Bologna, Italy; mario.vozza@ismn.cnr.it

* Correspondence: nele@unina.it

Abstract: Welding is one of the most complex industrial processes because it is challenging to model, control, and inspect. In particular, the quality inspection process is critical because it is a complex and time-consuming activity. This research aims to propose a system of online inspection of the quality of the welded items with gas metal arc welding (GMAW) technology through the use of neural networks to speed up the inspection process. In particular, following experimental tests, the deviations of the welding parameters—such as current, voltage, and welding speed—from the Welding Procedure Specification was used to train a fully connected deep neural network, once labels have been obtained for each weld seam of a multi-pass welding procedure through non-destructive testing, which made it possible to find a correspondence between welding defects (e.g., porosity, lack of penetrations, etc.) and process parameters. The final results have shown an accuracy greater than 93% in defects classification and an inference time of less than 150 ms, which allow us to use this method for real-time purposes. Furthermore in this work networks were trained to reach a smaller false positive rate for the classification task on test data, to reduce the presence of faulty parts among non-defective parts.

Keywords: GMAW; neural networks; quality inspection; artificial intelligence; machine learning



Citation: Nele, L.; Mattera, G.; Vozza, M. Deep Neural Networks for Defects Detection in Gas Metal Arc Welding. *Appl. Sci.* **2022**, *12*, 3615. <https://doi.org/10.3390/app12073615>

Academic Editor: Krzysztof Koszela

Received: 22 February 2022

Accepted: 29 March 2022

Published: 2 April 2022

Publisher's Note: MDPI stays neutral with regard to jurisdictional claims in published maps and institutional affiliations.



Copyright: © 2022 by the authors. Licensee MDPI, Basel, Switzerland. This article is an open access article distributed under the terms and conditions of the Creative Commons Attribution (CC BY) license (<https://creativecommons.org/licenses/by/4.0/>).

1. Introduction

Gas metal arc welding (GMAW), shown in Figure 1, is a very complex process that is difficult to model and control due to the complexity of the involved phenomena. Moreover, it is very difficult to perform an inspection in progress because it is actually only possible at the end of the welding operation. However, artificial intelligence techniques can be used for this purpose [1,2]. The welding process is difficult to control, due to the different physics of the system, such as mechanical, electrical, and thermal, and also for this case, artificial intelligence can be a way to solve the problem [3].

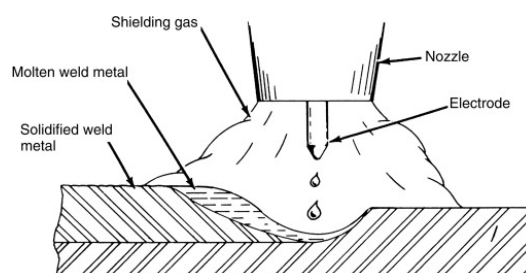


Figure 1. GMAW process.

This work is focused on the inspection phase, which is critical because, in case of a detected defect, there will be the need to rework the realized seam. The problem is even

more significant for multi-pass welding, where the quality of the previous pass affects the next one. Moreover, this results in a productivity problem since repairing a defective joint involves considerable costs in terms of resources and time.

Review of GMAW Process and Defects

The welding process is based on a localized heat source that allows the melting of the materials. The intensity of the heat source determines the thermal transient and the mode of melting and re-solidification of the joint, on which the quality depends. The formula for specific heat input is as follows:

$$Q = \frac{I * V}{v_t} * \eta \quad \left[\frac{\text{J}}{\text{mm}} \right] \quad (1)$$

The basic parameters to be monitored in a GMAW process are the welding speed v_t , the generator voltage V , and the arc-current I . In particular, the arc current is strongly variable with contact to workpiece distance (CTDW), wire feed rate, and wire properties, such as diameter and material [4] since the generator characteristic for this process is generally flat voltage, shown in Figure 2 [5].

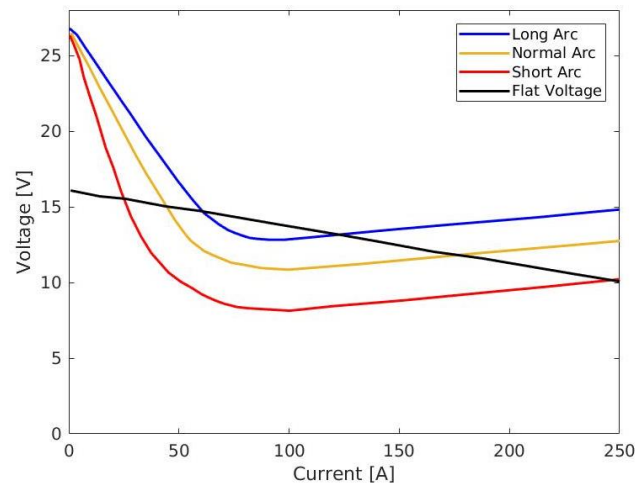


Figure 2. Self-autoregularization of arc current with constant voltage characteristics.

Defects in welding are principal of two types:

- Metallurgical discontinuities, which are problematic primarily due to the drop in mechanical properties of the joint and are typically identified through nondestructive testing.
- Metallurgical inhomogeneity, which is more complex to identify and assess.

Typical defects include cracks, inclusions, and lack of penetration [6,7]. These defects are associated with unsuitable process parameters and, therefore, unsuitable specific heat. For example, if the specific heat is too low due to low current or high torch speed. In this case, there may be a lack of fusion of the edges to be welded or a lack of penetration, while high values of specific heat, associated with a low torch speed, may lead to the presence of cracks or metallurgical in-homogeneity. An inadequate value of specific heat supplied to the weld bead can also lead to the birth of inclusions, such as gaseous inclusions, which consist of gas entrapment in the weld pool due to too fast cooling associated with too high welding speeds. In the literature, a strong correlation between process parameters and defects is presented. Wei et al. showed the correlation between arc current and porosity [8]. Pal shows that current and voltage, which are correlated with acoustic emissions [9], are correlated with the depth of penetration and geometry aspect of the joint for a P-GMAW [10]. Additionally, the temperature and geometry of the arc are correlated with defects, as shown by Sreedhar [11] and Brobeg [12]. It is not always easy to check for defects in the joints, and

this is a long and time-consuming job, especially when components are standardized and produced in large quantities. A sample check is carried out only on a few random samples in some sectors. In this case, artificial intelligence can be a viable method to evaluate the correct quality level for all components, including the items that skip the inspection stage. This is possible because the process parameters are directly involved in the defects rising, and these are all easily measurable. Shin et al. used different network architectures to correlate current and arc voltage to porosity, with an accuracy between 66–89% [13]. During gas metal arc welding, assuming that the generator has a flat voltage characteristic, slight variations in arc length lead to non-negligible fluctuations in the current affecting the arc: as the arc length increases, the current decreases, and vice versa, as seen in Figure 2.

In this case, the operator's task—a human or a robotic arm—is to change parameters, such as the torch's height from the workpiece, to bring these values back into range. This self-regulating characteristic of the electric arc leads to variations in current and, therefore, in the specific heat input supplied to the joint, which may cause defects in the items.

The Welding Procedure Specification (WPS) is a document that describes welding procedures and contains all the information needed to make quality welds. In the WPS, depending on the workpiece material, type of weld, and thickness, the welding parameters are provided, leading to a specific value for the heat input provided to it. For this work, information regarding process parameters such as current, voltage, and welding speed were collected from welds of different thickness in multi-pass welding, shown in Figure 3.

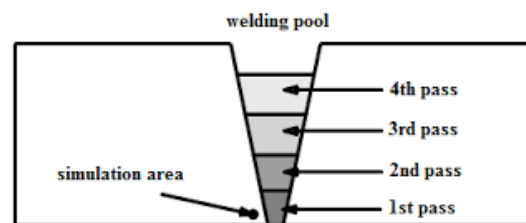


Figure 3. Multi-pass welding.

These values were compared with those in the WPS, which defines the best process parameters to reach a good quality of welded joint and that is obtained following experiments. The obtained errors were used to train a neural network. To the author's best knowledge, this approach, inspired by control theory, is innovative in this field and helps training and so the performance because the error is a better variable to understand the meaning of the “high or low” process parameter, which is correlated to defects in the way presented before. The labels, necessary to train the supervised network, were obtained through non-destructive tests (NDTs), specifically ultrasonic and penetrant liquids tests, and we found the type and location of defects in the workpiece. In particular, ultrasonic testing allows us to find the depth at which a defect can be traced, which is the key to creating the labels for the multi-pass GMAW process. The schematic procedure used for this work is shown in Figure 4.

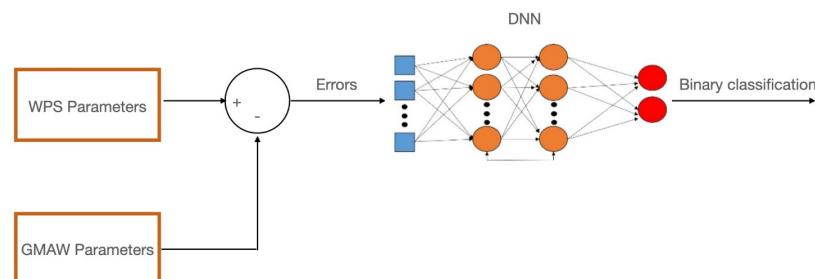


Figure 4. Procedure of training used in this work.

2. Materials and Methods

2.1. A Brief Summary of Artificial Neural Networks

Artificial neural networks (ANNs) are widely used in industry due to their ability to solve complex problems, such as image classification [14], audio classification [15], reinforcement learning [16], and to find patterns among a large amount of data [17]. Moreover, ANNs possess the ability to approximate any continuous function [18], and thus it is also used to derive models from data [19]. The basic structure of an ANN is a single layer perceptron (SLP) which consists of an input and an output layer, and it is the simplest ANN model, as shown in Figure 5.

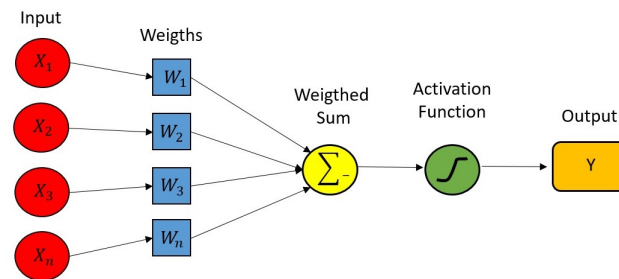


Figure 5. Single layer perceptron architecture.

However, this model cannot describe complex problems, so nowadays multilayer perceptron models (MLP) are mainly used, including more hidden layers between the input and output layers allow to overcome the limitations SLPs. The structure of an ANN MLP is shown in Figure 6.

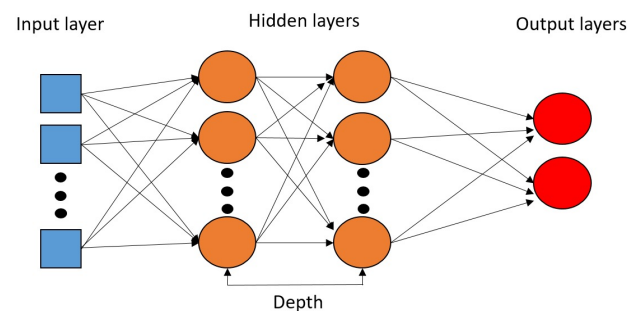


Figure 6. Multilayer perceptron architecture.

The structure of an MLP, often called fully connected neural networks, is composed of many computational units defined as neurons, all connected through connections called weights. In particular, all the neurons of layer i are connected to those of layer $i - 1$. Before passing to the next layer, the neuron's output is eventually added with a constant (bias), which allows translating the value of a certain quantity. This output is passed through a non-linear activation function, a fundamental part that allows the neural network to approximate any continuous non-linear function.

Finding a useful network architecture for a specific task is not a trivial problem. It is a programmer's job to choose the best architecture, network depth, number of neurons for each hidden-layers and activation function. Usually, this is done following a trial-and-error approach. It is also equally important to choose the optimization algorithm and the cost function to minimize that allows the neural network to learn the weights and biases and all hyperparameters like learning rate and regularization constants. For this purpose, gradient-based techniques of optimization find great use [20].

2.2. Development Workflow

In this work deviations of processing values from the optimal values described in the WPS were used as inputs to the neural network. Specifically, four inputs were used:

$$e_1 = \Delta v_{tmean} = v_{tmean}^{WPS} - v_t^{eff} \quad (2)$$

$$e_2 = \Delta I_{max} = I_{max}^{WPS} - I_{eff} \quad (3)$$

$$e_3 = \Delta I_{min} = I_{min}^{WPS} - I_{eff} \quad (4)$$

$$e_4 = \Delta V_{mean} = V_{mean}^{WPS} - V_{eff} \quad (5)$$

The output layer was characterized by a binary classification problem that associates 1 with adequate quality joints, as shown in Figure 4. In this work, we considered ten workpieces of 1 m of the length of a multi-pass gas metal arc welding with three different passes. We decided to slice each workpiece into 20 parts and acquire labels every 5 cm with NDT. With a sample time of $T_s = 225$ ms, which is constrained from Miller acquisition hardware at a maximum of 0.1 s (Insight ArcAgent), we obtain 2655 samples that we used to train the neural network. The dataset is built by imposing a correspondence between the data acquired on each part section and the NDT result in the same section of 5 cm for all three passes of multi-pass welding. The hypothesis is that all data acquired in the same section have the same label. The references, namely the WPS, are known before the process and are equal for all pass and workpiece samples. NDTs are used to localize the defect (distance from the starting point and depth for identifying the pass) and correlate it with acquired sample parameters.

2.2.1. Case Study and Data Collection

The case study under consideration is based on the realization of welds on bases for an offshore plant on an FPSO vessel. No special materials were used for this work; almost all of the basement is made of S355J2 structural steel.

Multi-pass welds were performed using a Miller XMS 425 MPa in Figure 7 and a gas composed of 82% of argon and 18% carbon dioxide. The wire, with a 1.2 mm diameter, is AWS certified as A5.18:ER70S-6.



Figure 7. Miller XMS 425 MPa welding machine.

Miller Insight Core software was used to monitor welding operations and subsequent collection of welding parameters; this software allows monitoring in real-time and storing all the process parameters on a cloud. Together with the WPS, this data was exported in excel format and then pre-processed in a python environment.

Ultrasonic, magentoscopic, and penetrant liquids tests were performed on the welds. Figure 8 shows an image of one of the tests performed using penetrant liquids, which

revealed the presence of a crater. Moreover, through an ultrasound inspection, it was possible to highlight a lack of fusion at a certain depth from the surface, corresponding to a certain welding pass to which certain welding parameters were associated. In this way, it was possible to assign labels to each welding pass whose process values were known. All of this information has been collected in a single file, which followed a pre-processing step in Python.

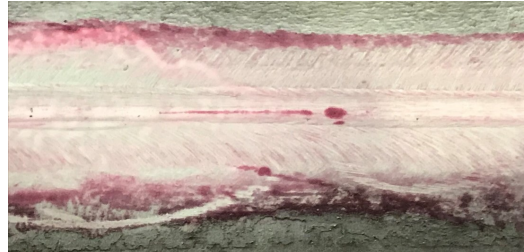


Figure 8. Penetrant liquid inspection result.

Pre-processing of the data involved scaling of the values to reference values for all process variables, to guarantee the same scale to all variables in input in neural network:

$$e_i = \frac{r - v_i}{r} \quad (6)$$

where r is the reference and v_i the actual value of variable. So for each weld the scale errors were collected in a 4×1 vector of features, and Equations (2)–(5) become:

$$e_1 = \Delta v_{tmean} = \frac{v_{tmean}^{WPS} - v_t^{eff}}{v_{tmean}^{WPS}} \quad (7)$$

$$e_2 = \Delta I_{max} = \frac{I_{max}^{WPS} - I_{eff}}{I_{max}^{WPS}} \quad (8)$$

$$e_3 = \Delta I_{min} = \frac{I_{min}^{WPS} - I_{eff}}{I_{min}^{WPS}} \quad (9)$$

$$e_4 = \Delta V_{mean} = \frac{V_{mean}^{WPS} - V_{eff}}{V_{mean}^{WPS}} \quad (10)$$

where V^{WPS} is the voltage reported in the WPS and V_{eff} is the measured voltage. The same is for the others parameters like welding speed v_t and current I . Following the non-destructive tests, it was possible to associate the corresponding label with each feature vector corresponding to the single welding pass, as mentioned before.

2.2.2. Choosing an Architecture

The chosen architecture is a multi-layer or fully connected network with a 4×1 vector as the input layer and a binary value as output. For this reason, the activation function of the output layer will be a sigmoid, in Figure 9, since we solve a binary classification problem [21].

The sigmoid activation function is defined as follows, where t is the input parameter:

$$\sigma(t) = \frac{1}{1 + e^{-t}} \quad (11)$$

This function allows us to transform an input between $[-\infty, +\infty]$ into a new one between $[0, 1]$. We associate with 1 the case of welding without defects. Probability $1-p$ is instead the one that describes the probability that the input feature vector is associated with a label 0.

Concerning the depth of the neural network, two different solutions have been studied. Architecture A consists of three hidden layers composed of [300, 200, 100] neurons in the different layers, where Architecture B consist in two hidden layer composed of [300, 100] neurons. These solutions are shown in Figures 10 and 11.

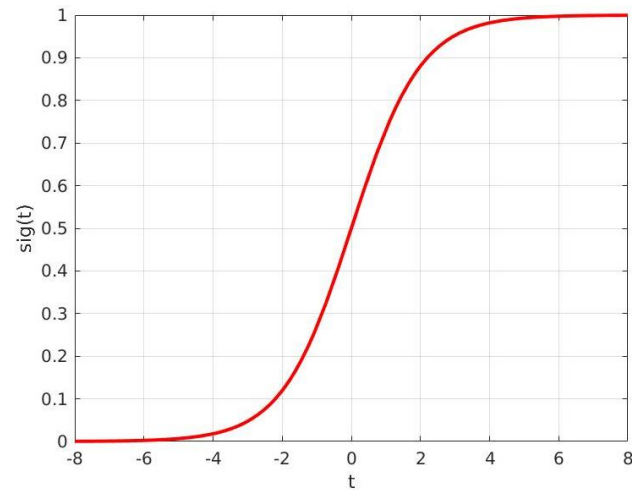


Figure 9. Sigmoid function.

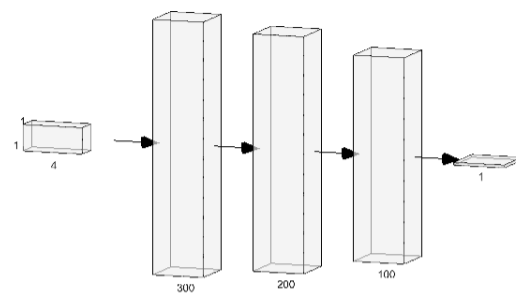


Figure 10. Architecture A.

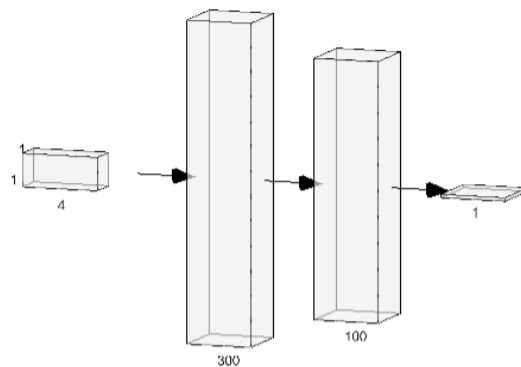


Figure 11. Architecture B.

The activation function chosen for each layer is a hyperbolic tangent, a function similar to sigmoid, shown in Figure 12.

$$\sigma(t) = \frac{e^t - e^{-t}}{e^t + e^{-t}} \quad (12)$$

This function allows us to transform an input between $[-\infty, +\infty]$ into a new one between $[-1, 1]$, and is frequently used in ANN architectures [21].

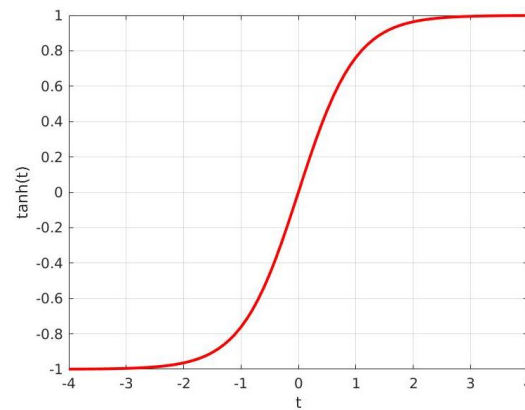


Figure 12. Hyperbolic tangent activation function.

For each layer, uniform Glorot distribution [22] was chosen as the initialization method for the weights because it is the most performing on activations functions sigmoid-like, such as the hyperbolic tangent function [23].

$$\mu = 0; \sigma = \sqrt{\frac{2}{n_i + n_o}} \quad (13)$$

Finally between in the layer $[n - 1]$ is add a dropout layer. The function of the dropout, whose results are shown in Figure 13, is to reduce the probability of overfitting by deleting random layer with a certainly probability [24].

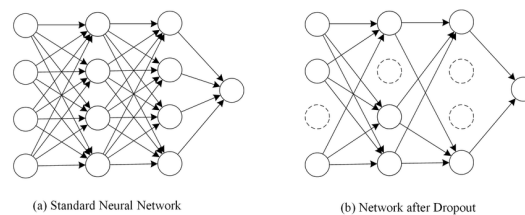


Figure 13. Dropout layer: (a) a standard neural network (b) the same network after dropout.

2.2.3. Training

For the Architecture “A” there are 81,901 parameters to train, while for Architecture “B” 31,701. For the neural network training, a batch size of 64 was used to accelerate the training phase. The usage of the batches can be seen from the oscillation of the loss and accuracy graphs [25]. The optimization algorithm used is adaptive momentum estimation [26]. The learning rate is the most important hyper-parameter for training a neural network. Typically, the lrDecay technique is used to improve training performance and overcome problems due to the convexity of cost functions, reducing overfitting. You et al. [27] showed that an initially large learning rate suppresses the storage of noisy data while decaying the learning rate improves the learning of complex patterns. Therefore, a learning rate of $lr_{ini} = 0.1$ and an exponential decay law were used:

$$lr = lr_{ini} * e^{-(step/decay)} \quad (14)$$

The main features of the training phase are summarized in Table 1.

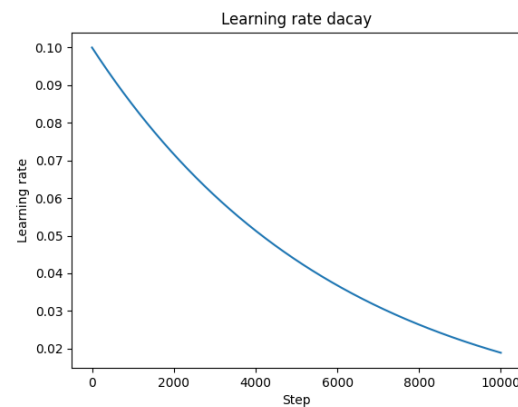
Figure 14 shows the exponential decay curve with $decay = 6000$. With the chosen decay value, at the end of training, about 10,000 steps, the value taken by $lr = 0.02$.

An NVIDIA GeForce GTX 1650—GDDR5 was used as the target for the training and subsequent inference phase, whose characteristics are shown in Table 2:

Training and testing of the neural network were performed using the Tensorflow library [28].

Table 1. Summary of hyper parameters of ANN.

Total samples	2655
Batch size	64
Initial learning rate (lr_{ini})	0.1
Decay	6000
β_1	0.9
β_2	0.99
ϵ	1×10^{-7}
Epochs	300
Step per epoch	35
Training size (% on the total)	85%
Validation size (% on the total)	10%

**Figure 14.** Exponential decay of learning rate.**Table 2.** NVIDIA GeForce GTX 1650 characteristics.

Core NVIDIA CUDA	896
Boost Clock (MHz)	1665
Base Clock (MHz)	1485
Memory speed (Gbps)	8
Compute capability	7.5
Microarchitecture	Turing

3. Results

In the following, the loss function and accuracy trends during the training phase for the training and validation dataset are shown. Finally, for each solution, we report the confusion matrix associated with the test dataset, 5% of the total, and the inference times for each solution.

3.1. Architecture A

Figures 15 and 16 show the trends of the loss function and the accuracy of varying the epochs.

The results obtained at the end of the training and testing phase are shown in Table 3:

Figure 17 shows the confusion matrix showing that 4.4% of the defective joints were classified as compliant while 2% of the compliant joints were classified as defective.

3.2. Architecture B

Figures 18 and 19 show the trends of the loss function and the accuracy of varying the epochs for Architecture B.

The results obtained at the end of the training and testing phase are shown in Table 4:

Figure 20 shows the confusion matrix showing that 1.5% of the defective joints were classified as compliant while 3.8% of the compliant joints were classified as defective.

Architecture B is the best solution due to the reduced inference time and the fewer non-conforming joints labeled as conforming, ensuring better performance and quality prediction confidence.

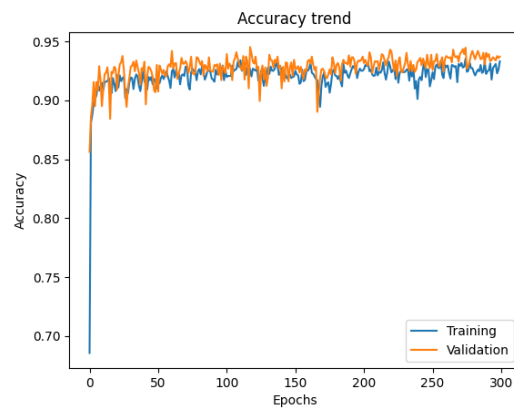


Figure 15. Accuracy trend for Architecture A.

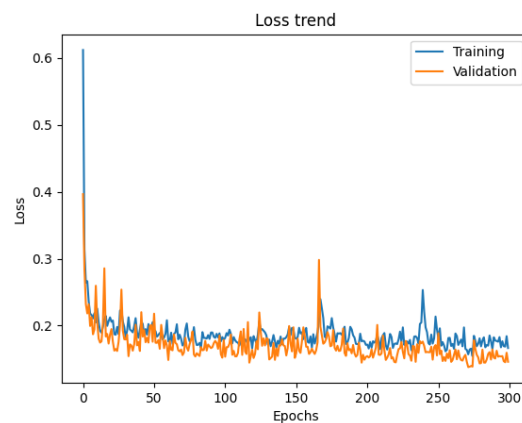


Figure 16. Loss trend for Architecture A.

Table 3. Principal results of Architecture A.

Final validation loss	0.16
Final training loss	0.18
Test accuracy	93.6%
Inference time (ms)	123.42

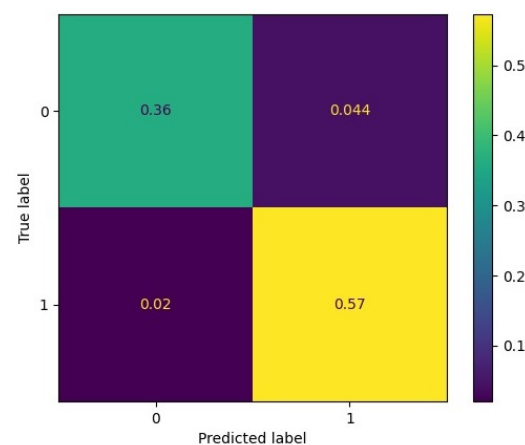


Figure 17. Confusion matrix of Architecture A.

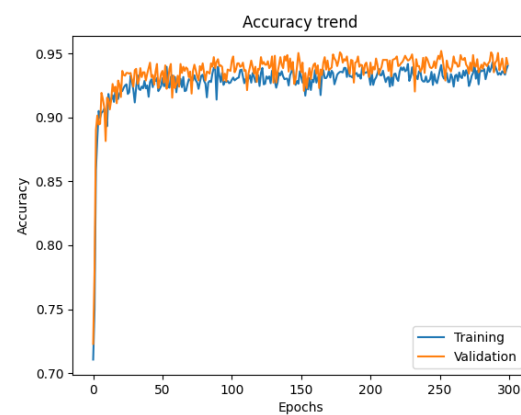


Figure 18. Accuracy trend for Architecture B.

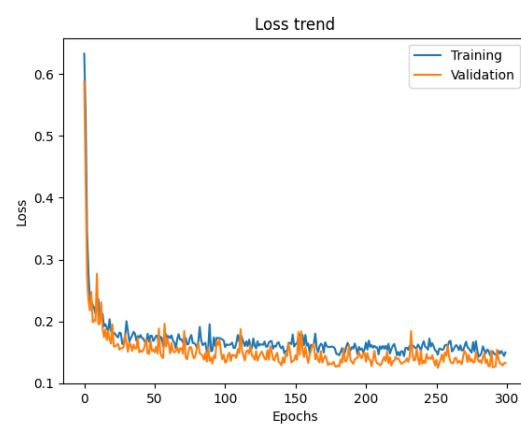


Figure 19. Loss trend for Architecture B.

Table 4. Principal results of Architecture B.

Final validation loss	0.13
Final training loss	0.15
Test accuracy	94.7%
Inference time (ms)	93.9

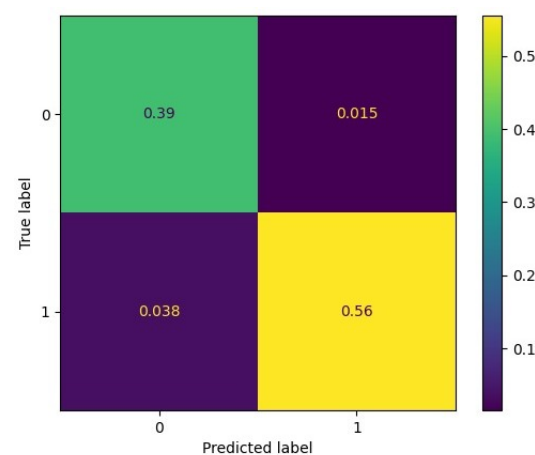


Figure 20. Confusion matrix of Architecture B.

4. Conclusions and Future Developments

In this work, the welding parameters corresponding to each pass during multi-pass GMAW welding of offshore platform bases performed by a robotic axis were monitored.

Subsequently, through non-destructive testing, it was possible to label the welds that did not show any defect, using different NDTs to find defects of different topologies. Once the dataset was generated, it was followed by a pre-processing activity, which led to obtaining four characteristic deviations of the welding parameters, acquired from the process with a sample rate of 225 ms, from those defined by the Welding Procedure Specification. With these deviations, a neural network with one or two hidden layers was trained, and the results were compared. At the end of the training phase, the neural network B presented 97% accuracy for joint classification. The proposed method is a novelty because is not only based on the usual data-driven approach of deep neural networks but is inspired by control theory with the concept of error. This new approach guarantees better results compared to other works, like that of Shin et al. [13], who proposed a similar approach with an accuracy of less than 90% for porosity detection. Furthermore, this network is also trained on different kinds of defects. These results represent a starting point for developing a more robust online quality control system for GMAW, which will be developed by integrating a camera in the inspection loop, which will allow the detection of other defects, including geometric ones during the welding process. However, in this work, only one type of material and wire were considered and is based on one type of WPS. To guarantee a generalization to any GMAW process more experiments must be conducted because the same error should not have the same influence on different materials, so other inputs could be considered, such as wire and workpiece material, joint temperature, gas flow rate, etc. The next step of this work could be the integration of other information like images and new experiments that lead to improving the performance and generalization capability of the network. After this, it will be possible to use the results in real-time for various purposes, such as the development of a new control logic for the feeder unit and robotic axis to adjust the parameters with the aim to avoid weld defects, which can work in the same loop with an intelligent monitoring system.

Author Contributions: Data curation, L.N., G.M. and M.V.; Formal analysis, L.N. and G.M.; Investigation, G.M.; Methodology, G.M. and M.V.; Software, G.M. and M.V.; Supervision, L.N. All authors have read and agreed to the published version of the manuscript.

Funding: This research received no external funding.

Informed Consent Statement: Not applicable.

Data Availability Statement: Data are available under request to corresponding author.

Conflicts of Interest: The authors declare no conflict of interest.

Abbreviations

The following abbreviations are used in this manuscript:

WPS	Welding Procedure Specification
GMAW	Gas Metal Arc Welding
ANN	Artificial Neural Networks

References

1. Xia, C.; Pan, Z.; Polden, J.; Li, H.; Xu, Y.; Chen, S. Modelling and prediction of Surface roughness in wire arc additive manufacturing using machine learning. *J. Intell. Manuf.* **2021**, 1–16. [\[CrossRef\]](#)
2. Deng, H.; Cheng, Y.; Feng, Y.; Xiang, J. Industrial Laser Welding Defect Detection and Image Defect Recognition Based on Deep Learning Model Developed. *Symmetry* **2021**, *13*, 1731. [\[CrossRef\]](#)
3. Xia, C.; Pan, Z.; Zhang, S.; Li, H.; Xu, Y.; Chen, S. Model-free adaptive iterative learning control of melt pool width in wire arc additive manufacturing. *Int. Adv. Manuf. Technol.* **2020**, *110*, 2131–2142. [\[CrossRef\]](#)
4. Pan, J. Chapter 1: Dynamic behaviour of arc welding. In *Arc Welding Control*; Woodhead Publishing Ltd.: Cambridge, UK; CRC Press: Boca Raton, FL, USA, 2003; pp. 1–16.
5. Weman, L. Chapter 2: Equipment for MIG welding. In *MIG Welding Guide*; Woodhead Publishing Ltd.: Cambridge, UK; CRC Press: Boca Raton, FL, USA, 2006; pp. 29–35.

6. Weman, L. Chapter 9: Assessing weld quality in MIG welding. In *MIG Welding Guide*; Woodhead Publishing Ltd.: Cambridge, UK; CRC Press: Boca Raton, FL, USA, 2006; pp. 130–144.
7. Mathers, G. Weld defects and quality control. In *The Welding of Aluminium and Its Alloys*; Woodhead Publishing Ltd.: Cambridge, UK; CRC Press: Boca Raton, FL, USA, 2002; pp. 199–215.
8. Wei, E.; Farson, D.; Richardson, R.; Ludewig, H. Detection of Weld Surface Porosity by Statistical Analysis of Arc Current in Gas Metal Arc Welding. *J. Manuf. Process.* **2001**, *3*, 50–59. [[CrossRef](#)]
9. By, J.; Johnson, A.; Carlson, N.M.; Smartt, H.B.; Clark, D.E. Process Control of GMAW: Sensing of Metal Transfer Mode. *Weld. J.* **1991**, *70*, 91.
10. Pal, K.; Bhattacharya, S.; Pal, S.K. Investigation on arc sound and metal transfer modes for on-line monitoring in pulsed gas metal arc welding. *J. Mater. Process. Technol.* **2002**, *210*, 1397–1410. [[CrossRef](#)]
11. Sreedhar, U.; Krishnamurthy, C.V.; Balasubramaniam, K.; Raghupathy, V.D.; Ravisankar, S. Automatic defect identification using thermal image analysis for online weld quality monitoring. *J. Mater. Process. Technol.* **2012**, *212*, 1557–1566. [[CrossRef](#)]
12. Brobeg, P. Surface crack detection in welds using thermography. *NDT & E Int.* **2013**, *57*, 69–73. [[CrossRef](#)]
13. Shin, S.; Jin, C.; Yu, J.; Rhee, S. Real-Time Detection of Weld Defects for Automated Welding Process Base on Deep Neural Network. *Metals* **2020**, *10*, 389. [[CrossRef](#)]
14. Du, R.; Xu, Y.; Hou, Z.; Shu, J.; Chen, S. Strong noise image processing for vision-based seam tracking in robotic gas metal arc welding. *Int. J. Adv. Manuf. Technol.* **2019**, *101*, 2135–2149. [[CrossRef](#)]
15. Nanni, L.; Maguolo, G.; Brahnam, S.; Paci, M. An Ensemble of Convolutional Neural Networks for Audio Classification. *Appl. Sci.* **2021**, *11*, 5796. [[CrossRef](#)]
16. Jin, Z.; Li, H.; Gao, H. An intelligent weld control strategy based on reinforcement learning approach. *Int. J. Adv. Manuf. Technol.* **2019**, *100*, 2163–2175. [[CrossRef](#)]
17. Chiroma, H.; Abdullahi, U.A.; Alarood, A.A.; Gabralla, L.A.; Rana, N.; Shuib, L.; Hashem, I.A.; Gbenga, D.E.; Abubakar, A.I.; Zeki, A.M.; et al. Progress on Artificial Neural Networks for Big Data Analytics: A Survey. *IEEE Access* **2019**, *7*, 70535–70551. [[CrossRef](#)]
18. Hornik, K. Approximation capabilities of multilayer feedforward networks. *Neural Netw.* **1991**, *4*, 251–257. [[CrossRef](#)]
19. Selmic, R.R.; Lewis, F.L. Neural-network approximation of piecewise continuous functions: Application to friction compensation. *IEEE Trans. Neural Netw.* **2002**, *13*, 745–751. [[CrossRef](#)]
20. Ojha, V.K.; Abraham, A.; Snášel, V. Metaheuristic design of feedforward neural networks: A review of two decades of research. *Eng. Appl. Artif. Intell.* **2017**, *60*, 97–116. [[CrossRef](#)]
21. Rasamoelina, A.D.; Adjailia, F.; Sinčák, P. A Review of Activation Function for Artificial Neural Network. In Proceedings of the IEEE 18th World Symposium on Applied Machine Intelligence and Informatics (SAMII), Herlany, Slovakia, 23–25 January 2020; pp. 281–286. [[CrossRef](#)]
22. Bengio, Y.; Glorot, X. Understanding the difficulty of training deep feed forward neural networks. In Proceedings of the International Conference on Artificial Intelligence and Statistics, Sardinia, Italy, 13–15 May 2010; pp. 249–256.
23. Datta, L. A Survey on Activation Functions and their relation with Xavier and He Normal Initialization. *arXiv* **2020**, arXiv:abs/2004.06632.
24. Srivastava, N.; Hinton, G.; Krizhevsky, A.; Sutskever, I.; Ruslan, S. Dropout: A Simple Way to Prevent Neural Networks from Overfitting. *J. Mach. Learn. Res.* **2014**, *15*, 1929–1958. Available online: <http://jmlr.org/papers/v15/srivastava14a.html> (accessed on 21 February 2022).
25. Gao, F.; Zhong, H. Study on the Large Batch Size Training of Neural Networks Based on the Second Order Gradient. *arXiv* **2020**, arXiv:2012.08795.
26. Kingma, D.P.; Ba, J. Adam: A Method for Stochastic Optimization. *arXiv* **2014**, arXiv:1412.6980
27. You, K.; Long, M.; Wang, J.; Jordan, M. How does learning rare decay help modern neural networks? *arXiv* **2019**, arXiv:1908.01878.
28. Tensorflow. Available online: <https://www.tensorflow.org/> (accessed on 10 November 2021).